

# Influence of urban spatial morphology on air temperature variance

Guixin Zhang<sup>1,2,\*</sup>, Zhenchun Hao<sup>3</sup> and Shanyou Zhu<sup>2</sup>

<sup>1</sup>College of Hydrology and Water Resources, Hohai University, Nanjing 210098, China

<sup>2</sup>School of Geography and Remote Sensing, Nanjing University of Information Science and Technology, Nanjing 210044, China

<sup>3</sup>State Key Laboratory of Hydrology-Water Resources and Hydraulic Engineering, Hohai University, Nanjing 210098, China

**Urban spatial geometric morphology is one of the key factors that results in air temperature variance between urban and suburban sites or at different urban positions. Considering the Adelaide central urban area of South Australia as study area and using urban digital elevation model (DEM) data with a high spatial resolution and field measurement meteorological data, this study estimated the sky view factor (SVF), frontal area index (FAI), and accumulated absorbed solar irradiation (AASI) from the land surface; these parameters were used to discuss the influence of the land surface on air temperature and urban heat island (UHI) under an optimal scale. The results indicate that urban spatial morphological parameters of the visually neighbouring positions display an obvious effect on the spatial-temporal air temperature variance. The degree of influence of AASI on air temperature variance during daytime increases with the solar elevation angle. A difference was noted between the influence of SVF and FAI on the urban heat island at different times in summer and winter, in which the influence of SVF and FAI on nocturnal UHI is more significant, whereas the relationship during daytime is complex.**

**Keywords:** Air temperature, frontal area index, solar irradiation, sky view factor, urban heat island.

URBAN geometric characteristics such as street width, street direction, sides of the street and the nearby layout, and form, height and spacing of the buildings affect street ventilation and surface effective radiation. Therefore, these factors change the wind direction, heat distribution and micro-climate within the city<sup>1-5</sup>. This alteration is one of the key factors that causes the differences in air and land surface temperatures between urban and suburban areas. Oke established the relationship between the average sky view factor (SVF), the mean ratio of the height and the width of the street and the measured maximum urban heat island intensity (UHII)<sup>1</sup>. This previous study considered that the geometric features of a city are the fundamental reasons that control the urban heat island (UHI). In recent years, based on the characteristics of the

urban geometric structure, multiple studies have defined and calculated different urban spatial morphological parameters and then analysed the relationship of these parameters with the air temperature and UHII in different seasons and various regions<sup>3,5-9</sup>.

The majority of research in India and abroad has been performed by estimating the SVF, frontal area index (FAI) and their relationship with UHII, in which the research on the SVF is more common. Multiple study areas, including Hong Kong, have been selected to perform research on the SVF-UHII<sup>3,6-9</sup>. Results of the SVF with urban air temperature and the UHII show positive and negative correlations during daytime, and the relationships change with time and position; whereas the SVF has a significant negative correlation between SVF and UHII at night. Regarding studies on FAI and UHII, Chen *et al.* calculated the frontal area density (FAD) and SVF in the Hong Kong area and then simulated and analysed the UHI distribution and wind dynamic graph<sup>8</sup>. Wong *et al.* calculated the FAI under different spatial scales and discussed its relationship with the UHII retrieved from Advanced Spaceborne Thermal Emission and Reflection Radiometer (ASTER) image data<sup>10</sup>.

Most studies on related research are performed by correlating the SVF with UHII during the night while fewer systematic research studies investigate the relationship between the FAI and UHII, and the different influence of FAI and SVF on UHII in different seasons. During daytime, the temporal and spatial changes of city air temperature are closely related to the solar irradiation absorbed by the surface of the earth. Different urban morphologies and underlying surfaces might result in air temperature variances on the scale of an urban block, which requires further discussion.

Considering the central urban area of Adelaide, South Australia as study area and calculating urban morphological parameters such as SVF and FAI, the present study discusses the difference in the contribution of SVF and FAI to UHII at various times in summer and winter. A case study conducted during daytime is also selected as an example to analyse the different effects of solar irradiation absorbed by the land surface, SVF and FAI. From the urban spatial morphological perspective, this article discusses the influence of the layout of the buildings on

\*For correspondence. (e-mail: zgxyzsy@163.com)

urban air temperature distribution and UHI effect, which could bridge the correlation between climatology and the planner and provide strong scientific evidence for city planning and construction decisions.

### Study area and data

#### Study area

Adelaide, the capital of South Australia, is located on the south coast of Australia (Figure 1). Adelaide comprises the core of a metropolitan area that extends approximately 20 km from the east to west and approximately 90 km from the north to south. The city has a total population of 1.22 million<sup>11</sup>. The centre of the Adelaide metropolitan area is surrounded by a belt of parklands several hundred metres wide on all sides. Adelaide has a Mediterranean climate, which is damp and cold in winter and dry and hot in summer. The average maximum temperature is approximately 28°C in summer and 15°C in winter. The annual average temperature and rainfall are approximately 17.1°C and 528 mm respectively.

#### Data

The present study adopted half-hourly air temperature data from 19 stations measured from September 2010 to August 2011. Three-dimensional (3D) building data (Figure 1) and aerial imaging surface albedo data with a spatial resolution of 1 m covering the central business district (CBD) were used. Daily meteorological observation data from the Adelaide airport station were also included.

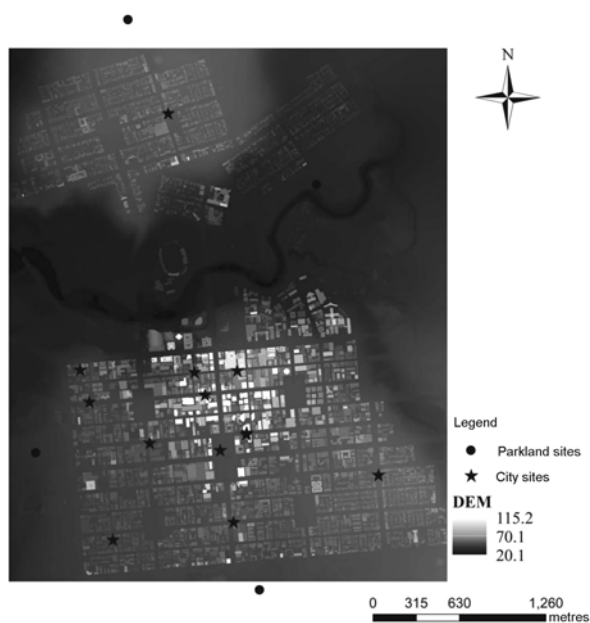


Figure 1. Three-dimensional building distribution and location of the field measurement stations.

### Methodology

#### Estimation of the sky view factor

SVF is defined as the ratio of the surface receiving (or emission) radiation and the entire hemisphere emission (or acceptance) radiation<sup>12</sup>. SVF is used to measure the extent of sky blocking in radiative transmission at a particular location. The SVF values range from 0 to 1 and change with position. A SVF value of 0 indicates that the sky is completely blocked and all radiation is intercepted, whereas a value of 1 indicates that the surface will receive (or emit) all radiation.

The methods used to estimate SVF are divided into four categories: analytical method, fisheye camera technology, computational estimations using 3D data and GPS signal estimations<sup>13</sup>. This study estimated the SVF with 3D raster data adopting the principles shown in Figure 2.

For point O, the algorithm divides the hemispheric radiating environment with radius R into equal slices by a rotation angle dα and searches for a pixel P<sub>i</sub> with the largest elevation angle β<sub>i</sub> along a particular direction. The SVF at point O is calculated on basis of eq. (1). In Figure 2, the shaded sky area cannot be seen from point O.

$$SVF = \sum \cos^2 \beta_i \cdot (d\alpha/2\pi), \tag{1}$$

$$\beta_i = \arctan(h(P_i)/r_i), \tag{2}$$

where β<sub>i</sub> is the maximum elevation angle in the certain search direction, h(P<sub>i</sub>) the height difference between point P<sub>i</sub> and O, and r<sub>i</sub> is the horizontal distance between point P<sub>i</sub> and O.

#### Calculation of the frontal area index

Building walls facing the wind impart drag on the air flow. The FAI, a measure of the frontal area per unit

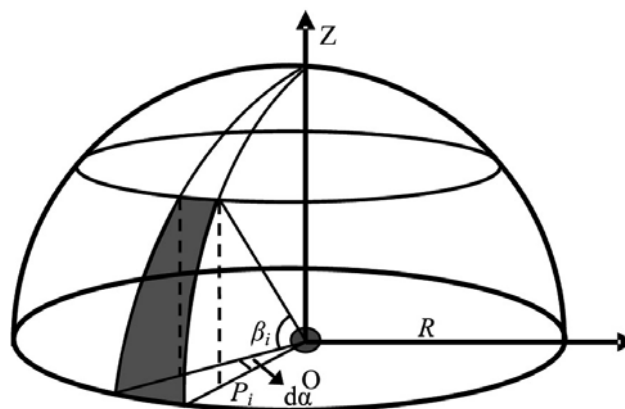


Figure 2. Illustration of the SVF calculation.

horizontal area, has been shown to be related to the surface roughness. FAI has been widely used in studies on UHI<sup>8</sup> and city ventilation environment<sup>14</sup>. The FAI is defined as the total area of buildings projected into the plane normal to the approaching wind direction ( $A(\theta)_{proj}$ ) divided by the plan area of the study site ( $A_T$ )<sup>15</sup> (Figure 3). The FAI is the accumulation of FAD for the entire building and is more capable of describing the dragging effect of buildings on the wind. A smaller FAI value indicates a lower dragging force of the building in the wind.

FAI is calculated using the equation

$$FAI(\theta) = \frac{A(\theta)_{proj}}{A_T}, \quad (3)$$

where  $\theta$  is the wind angle;  $A(\theta)_{proj}$  is the total area of the buildings projected into the plane normal to the approaching wind direction and  $A_T$  is the horizontal area corresponding to different research scales.

#### Calculation of the absorbed solar irradiation

Calculation process for ASI is shown in Figure 4, and estimation of  $ASI_t$  in a short period of time ( $t$ ), is shown in equation.

$$ASI_t = (I_b \cdot Bs + I_d) \cdot \Delta t \cdot (1 - \alpha), \quad (4)$$

where  $\alpha$  is the surface albedo and  $\Delta t$  is the calculation time step (0.5 h was used in this study). When the solar elevation angle ( $h$ ) is greater than the maximum elevation angle ( $\beta$ ), the calculation position is located in sunlight and  $Bs$  equals 1. The  $ASI_t$  then includes the direct solar radiation  $I_b$  and the scattering radiation  $I_d$ , otherwise  $Bs$  equals 0 and only considers the scattering solar irradiation  $I_d$  that reaches the surface. In eq. (4),  $(I_b \cdot Bs + I_d) \cdot \Delta t$  is an incidental solar radiation intensity

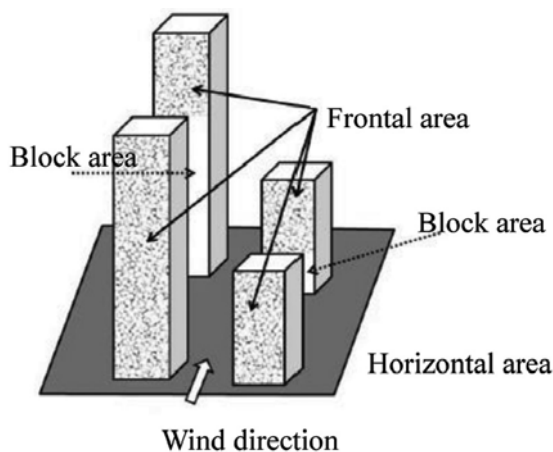


Figure 3. Illustration of the FAI calculation.

during a certain period of time, and  $I_b$  and  $I_d$  can be calculated with eqs (5) and (6) respectively.

$$I_b = I \cdot \tau_b, \quad (5)$$

$$I_d = [I \cdot \tau_d / (2 \cdot \sinh)] \cdot SVF, \quad (6)$$

$$I = I_0 \cdot F \cdot \sin h. \quad (7)$$

In these equations,  $I$  is the incoming solar radiation outside the atmosphere that does not consider the effect of the atmosphere and arrives at the horizontal level; the solar constant  $I_0$  is  $1367 \text{ W m}^{-2}$ ,  $F$  is the solar-earth correction coefficient, and  $\tau_b$  and  $\tau_d$  indicate the direct transmittance and scattering transmittance respectively, which are calculated using an empirical model<sup>16-18</sup>.

When the sun rises from  $t_0$  to a certain moment  $t$ , the accumulated absorbed solar irradiation by the surface ( $AASI_t$ ) can be expressed as

$$AASI_t = \sum_{t_i=t_0}^t ASI_{t_i}. \quad (8)$$

#### Relationship between urban spatial morphology parameters and air temperature variance

According to the principle of the land-atmospheric energy balance and radiation balance, air temperature variance in select positions is related to the heat absorbed and scattered by the land surface within the scope of a certain area and to the surrounding area heat flux variance significantly because of the effect of the horizontal air flow. According to the principle of the FAI calculation, the FAI value changes with the spatial scale ( $A_T$ ). Based on these two points, when analysing the influence of urban spatial morphology on the air temperature variance, we must first determine the suitable spatial scale and then consider the influence of spatial morphology parameters at neighbouring regions on air temperature variance of the centre area.

The key processes in this study are described as follows:

(1) *Expression of the air temperature variance characteristics.* For point  $i$ , air temperature difference between air temperature  $T_{a,i}^t$  at time  $t$  and  $T_{a,i}^{6:30}$  at the reference time 6:30 was calculated using eq. (9). In the time dimension,  $\Delta T_{a,i}^t$  can be used to present the regulation of air temperature changing with time; in the spatial dimension, when the air temperature  $T_{a,i}^{6:30}$  at different positions is known, air temperature distribution at time  $t$  could be derived from  $\Delta T_{a,i}^t$ .

$$\Delta T_{a,i}^t = T_{a,i}^t - T_{a,i}^{6:30}. \quad (9)$$

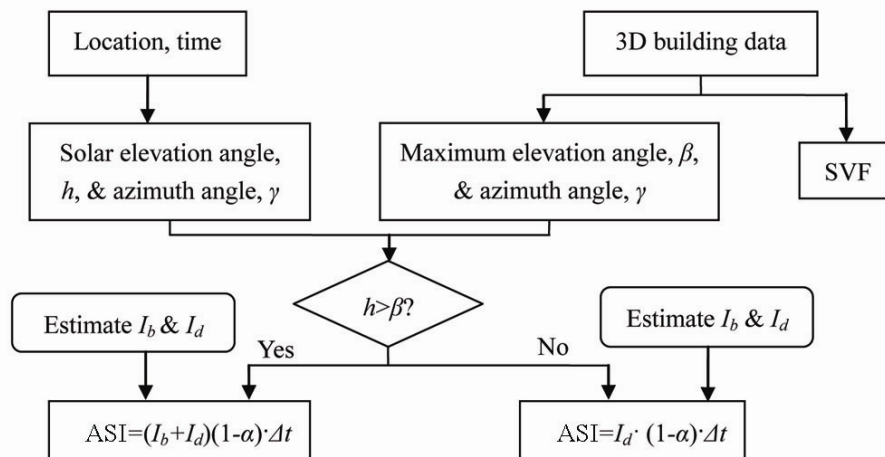


Figure 4. Calculation process for the absorbed solar irradiation.

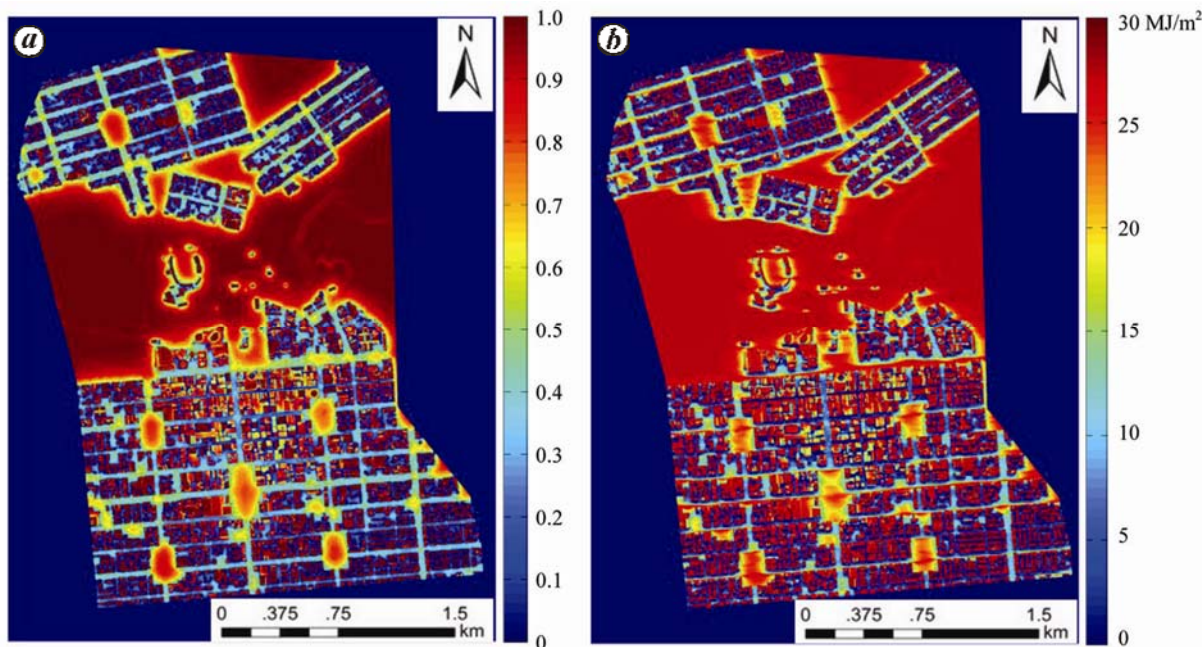


Figure 5. Distribution of the SVF and daily solar radiation during 6 March 2011. *a*, SVF distribution; *b*, Daily solar irradiation.

(2) *Urban heat island intensity calculation.* Using the average air temperature of six sites in the green belts of Adelaide as a reference, UHII of 13 sites in the urban area at half-hour intervals was computed from the equation.

$$UHII_{a,i}^t = T_{a,i}^t - \frac{1}{N} \sum_{j=0}^N T_{a,j}^t \quad (10)$$

In eq. (10),  $UHII_{a,i}^t$  is the UHII for site  $i$  at time  $t$ ;  $T_{a,i}^t$ , the measured air temperature for site  $i$ ;  $T_{a,j}^t$ , the referenced air temperature at site  $j$  in the green belts and  $N = 6$ .

(3) *Determining the optimal study spatial scale.* By analysing the changing rules in the relationship between the spatial morphology parameters and air temperature

for different spatial scales, the optimal spatial scale was determined.

(4) *Influence of the neighbouring region.* When considering the effects of the neighbouring pixel on air temperature of the central pixel location, we compared the following two cases. One case considers all neighbouring pixels, and the other case considers that the effect of the surrounding pixel on the central position was not included when the neighbouring pixel is not visible at the centre pixel through the sight analysis method.

(5) *Analysis of the relationship between the urban spatial morphology parameters and air temperature variance.* Using the daytime temperature variance on 6 March 2011 and the urban heat island intensity variance summer and winter at different times as the example, a single factor analysis combined with a multiple linear

statistical analysis methods was adopted to analyse the influence of different FAI, mean SVF ( $SVF_m$ ), and mean AASI ( $AASI_m$ ) on air temperature variance at time  $t$  at the optimal spatial scale.

## Results and discussion

### Analysis of the spatial distribution of the urban spatial morphology parameters

According to eq. (1), when the search radius  $R$  is larger and the azimuth spacing  $d\alpha$  is smaller, the calculation accuracy of the SVF and the computational time required will both be higher. In this study,  $d\alpha$  is set to  $1^\circ$  or  $2^\circ$ , and the search radius  $R$  is 50, 100, 150, 200, 250 and 300 m. We can then compare the precision of the SVF. Considering the balance between the calculation accuracy and speed,  $d\alpha$  is finally determined as  $2^\circ$  and the search radius  $R$  is 200 m, which are identical to the parameter values used in Chen *et al.*<sup>9</sup> and Unger<sup>19</sup>. Spatial distribution of SVF in the study area is shown in Figure 5 *a*.

Using Figure 4 and eq. (4), the spatial solar irradiation intensity on 6 March 2011 was calculated (Figure 5 *b*). At the Adelaide Airport weather station (lat.  $34.94^\circ\text{S}$ , long.  $138.52^\circ\text{E}$ ), the calculated result is  $25.2 \text{ MJ m}^{-2}$ , which is consistent with the measured daily solar irradiation intensity of  $26.0 \text{ MJ m}^{-2}$ . Comparing Figure 5 *a* and *b*, the surface received more solar irradiation intensity when the SVF is large, displaying a significant positive correlation. On city streets with similar SVFs, solar irradiation intensity in the north–south direction is significantly greater than that of the east–west direction. As the study area is located in the southern hemisphere, solar irradiation intensity on the north site of the east–west direction street is significantly lower than that of the south site because of the blocking effect of buildings.

### Determination of the optimal spatial scale

Unger studied the difference between the SVF and air temperature and found that compared to a single-point correlation<sup>3</sup>, the average SVF (within a certain range of space) displayed a much higher correlation with the air temperature. At 200 m spatial resolution, Nichol *et al.* found that the temperature variance above different land cover types can be accurately expressed in the city<sup>20</sup>. Wong *et al.* calculated the FAI for eight wind directions in Hong Kong Kowloon to analyse the urban heat island phenomenon at a 100 m spatial scale<sup>21</sup>. Thus, the effect of urban spatial morphology on the temperature depends on the spatial scale used in the analysis.

Considering that SVF, FAI and AASI display a high correlation with each other, the present study selects the SVF to determine the optimal spatial scale. The optimal spatial scale is determined by analysing the correlation

between the SVF and  $\Delta T_a^t$  under different spatial scales. Using the data measured on 6 March 2011 as an example, the correlation between the SVF and  $\Delta T_a^t$  changing with the spatial scale for six times is shown in Figure 6.

According to Figure 6, the relationship between the urban spatial morphology parameters SVF and air temperature variance changes significantly with the spatial scale at different times, which is consistent with the findings of Unger<sup>3</sup>, Nichol *et al.*<sup>20</sup> and Wong *et al.*<sup>21</sup>. Correlation between the SVF and air temperature variance increases gradually with the spatial scale when the spatial scale is smaller than 100 m (Figure 6). When the spatial scale exceeds 100 m, the correlation between SVF and  $\Delta T_a^t$  tends to be stable. When the spatial scale exceeds 240 m, the correlation begins to decline substantially. Thus, this study sets the optimal spatial scale as 100 m. Therefore, the FAI,  $SVF_m$  and  $AASI_m$  were estimated within  $100 \text{ m} \times 100 \text{ m}$  grids from the centre of the experimental site, and the influence of these parameters on the air temperature variance and UHII was then determined.

### Effects of neighbouring pixels at the optimal spatial scale

At the 100 m optimal spatial scale and using the data measured each hour of 6 March 2011 as an example,

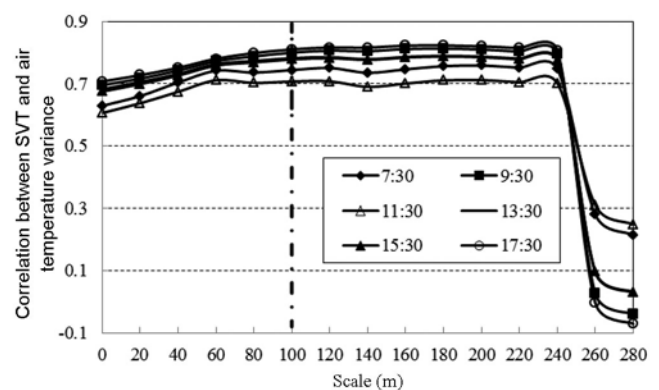


**Figure 6.** Correlation between the air temperature variance and SVF at different spatial scales.

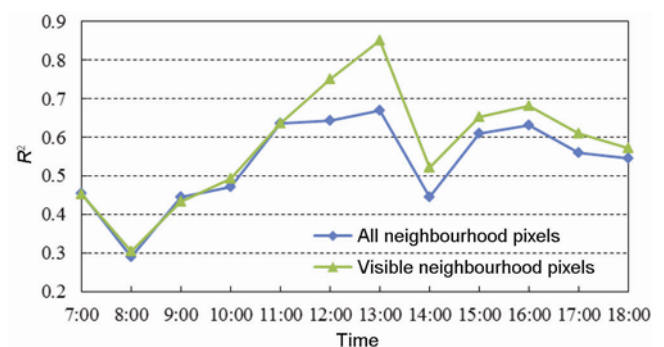


**Figure 7.** Influence of the neighbouring pixels on the correlation between air temperature and morphological parameters.

we calculated and compared the multivariate linear coefficient of determination between  $\Delta T_a^t$  and AASI, SVF, and FAI by considering all the neighbouring pixels and only the visually neighbouring pixels respectively. The results are shown in Figure 7. According to Figure 7, the influence of the spatial morphology parameters of visually neighbouring pixels on air temperature variance of the central position is more apparent when compared to all neighbouring pixels. Based on the physical mechanisms, heat and the energy differences between the visually neighbouring positions and the centre site tend to be balanced through the air flow because of the different spatial morphologies and underlying surface cover. However, the heat and the energy at the in visual positions are blocked by the middle buildings, displaying a relatively small effect on air temperature variance of the central pixels.

*Influence of urban spatial morphology on air temperature*

Considering the daytime data of 6 March 2011 as an example, we calculated  $\Delta T_a^t$  to express the spatial and

temporal variation of air temperature at moment  $t$  using eq. (9), the FAI, the mean accumulated absorbed solar irradiation (AASI<sub>m</sub>) and the mean sky view factor (SVF<sub>m</sub>) of the visually neighbouring pixels at the optimal 100-m scale. Correlation between the single factor and air temperature variance was then determined. The results are shown in Figure 8a. Moreover, the mean accumulated solar irradiation without considering the surface albedo was also calculated by changing eq. (4) and then its correlation was computed with the air temperature variance.

During daytime, solar irradiation is the main energy causing the near surface air temperature to rise and change. According to Figure 8a, the solar elevation angle gradually increases from morning to noon (7:00–13:00). The site at which the SVF is greater can receive more incident solar irradiation energy, and the air temperature rises faster. The air temperature spatial and temporal variation  $\Delta T_a^t$  is significantly positive and correlated to the AASI<sub>m</sub> and SVF<sub>m</sub>, and this positive correlation coefficient gradually increases with the solar elevation angle. This positive correlation coefficient is more than 0.7 during most of the time and can reach 0.8 at noon. From afternoon to sunset, the incident solar irradiation energy reaching the surface of the earth gradually decreases, the absorbed accumulated incident solar irradiation variance at different positions of the surface becomes smaller, and the near-surface air temperature spatial distribution variance is weaker. The positive correlation between  $\Delta T_a^t$  and the AASI<sub>m</sub> and SVF<sub>m</sub> is less than the midday periods and tends to gradually stabilize. As compared with the mean accumulated solar irradiation, the correlation between  $\Delta T_a^t$  and AASI<sub>m</sub> is larger with a mean value of about 0.12, which means the land surface absorbed solar irradiation has a greater influence on air temperature and this could be explained on the basis of the surface energy and radiation balance theory.

According to Figure 3 and eq. (3), the FAI value is identical under the condition of a symmetrical wind direction. In the case analysis, the wind speed varies from 4 to 6 m/s during daytime, and the wind direction is northeast during the morning hours, north at noon and southwest during afternoon. The overall wind direction was north–south in the day. Therefore, the FAI changes minimally with time. According to the definition of the FAI, larger FAI values represent better ventilation effects in the horizontal direction, better heat dissipation and a smaller magnitude of temperature change with time and space. A negative correlation is noted between  $\Delta T_a^t$  and the FAI. From Figure 8a, a significant negative correlation is noted at different times and changes little over time, notably after 9:00.

Variations in the correlation between  $\Delta T_a^t$  and the AASI<sub>m</sub> and SVF<sub>m</sub> with time are more consistent because of considering SVF in the calculation of the accumulated surface absorption of incident solar irradiation (Figure 8a). In a comprehensive analysis of the correlation

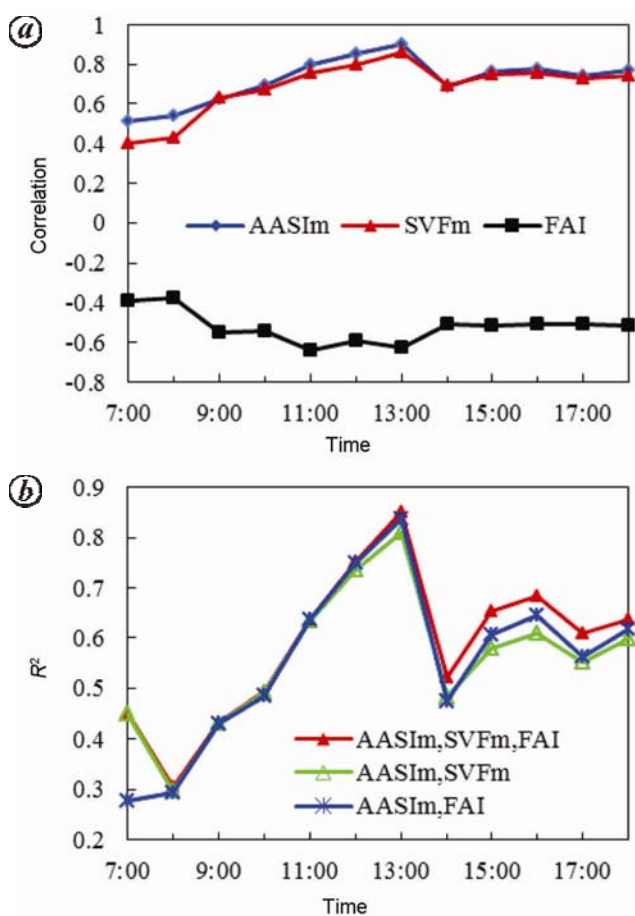


**Figure 8.** Correlation between air temperature variance and AASI, SVF, FAI changing with time. *a*, Single factor analysis; *b*, multiple linear statistical analysis.

between the three factors and the tempo-spatial variation of the air temperature, the  $AASI_m$  is more able to explain the air temperature variance change with space and time than the  $SVF_m$  and FAI. Based on Figure 8a and the corresponding analysis, further analyses on the relationship between multiple factors and the tempo-spatial variation of air temperature are shown in Figure 8b. According to Figure 8b, the coefficient of determination of the linear relationship developed in a single factor, multi-factor analysis changes minimally during the morning hours. The coefficient of determination of the multiple linear relationship on  $\Delta T_a^t - AASI_m$ ,  $SVF_m$ , and FAI gradually increases with the solar elevation angle and reaches a maximum value of 0.85 at 13:00. In the afternoon session, the surface heat absorption and scattering is at a similar level, and multiple factors can be used to better explain the spatial variation of temperature. The coefficients of determination in descending order are  $\Delta T_a^t - AASI_m$ ,  $SVF_m$ , FAI;  $\Delta T_a^t - AASI_m$ , FAI and  $\Delta T_a^t - AASI_m$ ,  $SVF_m$ ; these three factors can be used to explain approximately 60% of the tempo-spatial temperature variation characteristics.

*Summer and winter urban heat island intensity and its relationship with the spatial morphological parameters:* The surface-absorbed incoming solar radiation changes with seasons, time, and surface conditions. Accurate

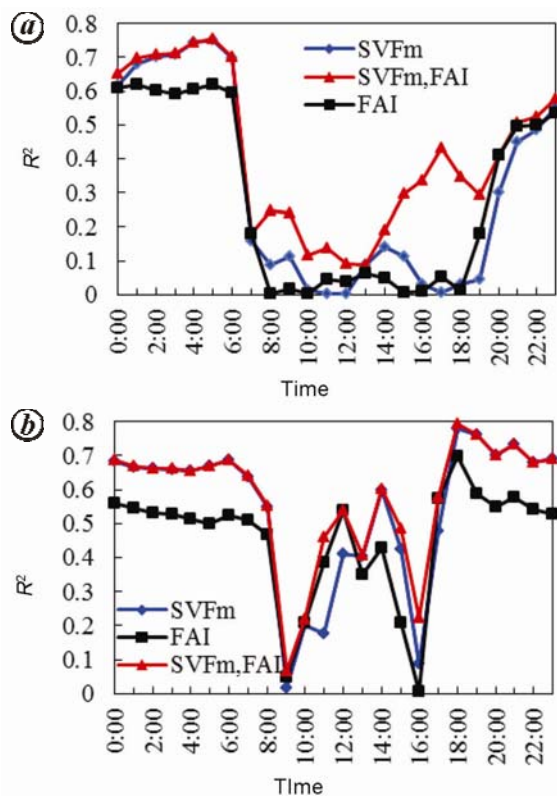


**Figure 9.** Correlation between UHII and SVF and FAI changing with time in summer and winter. *a.* Summer; *b.* Winter.

calculation of AASI at different times of the day for each season is difficult. Therefore, we only analysed the effect of SVF and FAI on the UHII during summer and winter. For each season, dates without rain are extracted from the Adelaide airport meteorological station data. This study used eq. (10) to calculate the UHII for each site at different times of the day and then averaged the UHII at different times for each site in summer and winter. According to the measured wind direction, we can calculate the occurrence probabilities of the on-the-hour wind direction, and use eq. (3) to calculate the FAI in different wind directions. We then weighted the average to obtain the FAI at different times. Figure 9 shows the coefficients of determination of a single factor, multi-linear relationship between the UHII and SVF and FAI at different times in the winter and summer respectively, for which the  $SVF_m$  indicates the mean SVF of the neighbouring pixels at the optical scale.

The influence of the SVF and FAI on UHII for different seasons at different times displays minimal differences (Figure 9). In the early morning hours (0:00–6:00), the influence of SVF on UHII is more pronounced than FAI, explaining more than 60% of the UHII change. The coefficient of determination between the SVF and UHII occasionally exceeds 0.7, and adding the FAI displays no additional significant change when analysing the influence on heat island intensity. During night (18:00–23:00), the influence of SVF and FAI on the heat island intensity differs in different seasons. During a summer night, the UHII–SVF correlation is less than the UHII–FAI, but is significantly greater during a winter night. The SVF can better explain the winter nighttime heat island phenomenon than the FAI. During daytime (6:00–18:00), the relationship between UHII and SVF and FAI is more complex. The correlation of SVF–UHII is greater after 13:00. When compared to a single factor, SVF and FAI can be used to better explain UHII during summer, but the coefficient of determination of UHII–SVF (FAI) is less than 0.3 most of the time. In winter, the difference between UHII and the two spatial morphological parameters is obscured. During the midday hours (11:00–15:00), the coefficient of determination between UHII and SVF (FAI) exceeds 0.4.

## Conclusion

By using the data covering 3D buildings with a high spatial resolution and measured meteorological data, we discussed the influence of urban spatial morphology on tempo-spatial variance of near-surface air temperature and UHII using the sky view factor, frontal area index and surface absorbed solar irradiation.

The main conclusions are as follows:

(1) When analysing the influence of urban spatial morphology on temporal and spatial temperature variance, we determine the optimal spatial scale for

different cities. This process accounts for the synthetic effects of the spatial morphology and land surface types in the surrounding area. For the study area of the Adelaide central urban area, the optimal spatial scale is 100 m when considering the influence of the visually neighbouring positions on temperature variance of the centre position could obtain a higher precision.

(2) For daytime temperature variance, the contribution and influence of the accumulated land surface absorbed solar irradiation increases with the solar elevation angle and gradually achieves a stable value.

(3) Influence of SVF and FAI on UHII is slightly different at different times in different seasons. This influence is more significant on the nocturnal UHII, and the relationship of UHII–SVF and UHII–FAI is complex during daytime.

1. Oke, T. R., Canyon geometry and the nocturnal urban heat island: comparison of scale model and field observations. *J. Climatol.*, 1981, **1**, 237–254.
2. Arnfield, A. J., Two decades of urban climate research: a review of turbulence, exchanges of energy and water, and the urban heat island. *Int. J. Climatol.*, 2003, **23**, 1–26.
3. Unger, J., Intra-urban relationship between surface geometry and urban heat island: review and new approach. *Clim. Res.*, 2004, **27**, 253–264.
4. Ding, W. W., Hu, Y. P. and Dou, P. P., Study of the interrelationship between urban pattern and urban microclimate. *Archit. J.*, 2012, **7**, 16–21 (in Chinese).
5. Liu, S. H. *et al.*, Multi-scale atmospheric boundary-layer and land surface physics process models. *Sci. Sin-Phys. Mech. Astron.*, 2013, **43**, 1332–1355.
6. Giridharan, R., Ganesan, S. and Lau, S. S. Y., Daytime urban heat island effect in high-rise high-density developments in Hong Kong. *Energ. Buildings*, 2004, **36**, 525–534.
7. Giridharan, R. *et al.*, Urban design factors influencing heat island intensity in high-rise high-density environments of Hong Kong. *Build. Environ.*, 2007, **42**, 3669–3684.
8. Chen, L. and Ng, E., Quantitative urban climate mapping based on a geographical database: A simulation approach using Hong Kong as a case study. *Int. J. Appl. Earth Obs.*, 2011, **13**, 586–594.
9. Chen, L. *et al.*, Sky view factor analysis of street canyons and its implications for daytime intra-urban air temperature differentials in high-rise, high-density urban areas of Hong Kong: a GIS-based simulation approach. *Int. J. Climatol.*, 2012, **32**, 121–136.
10. Wong, M. S. and Nichol, J. E., Spatial variability of frontal area index and its relationship with urban heat island intensity. *Int. J. Remote Sens.*, 2013, **34**(3), 885–896.
11. Australian Bureau of Statistics 2012. 2011 Census of population and housing; <http://www.abs.gov.au/websitedbs/censushome.nsf/home/Census>.
12. Watson, I. D. and Johnson, G. T., Graphical estimation of sky view factors in urban environments. *Int. J. Climatol.*, 1987, **7**, 193–197.
13. Zhu, S. Y. *et al.*, Influence of sky temperature distribution on sky view factor and its applications in urban heat island. *Int. J. Climatol.*, 2013, **33**, 1837–1843.
14. Ng, E. *et al.*, Improving the wind environment in high-density cities by understanding urban morphology and surface roughness: a study in Hong Kong. *Landscape Urban Plan.*, 2011, **101**, 59–74.
15. Burian, S. J., Velugubantla, S. P. and Brown, M. J., Morphological analyses using 3D building databases: Phoenix, Arizona. Los Alamos National Laboratory, 2002.
16. Liu, B. Y. and Jordan, R. C., The interrelationship and characteristic distribution of direct, diffuse and total solar radiation. *Sol. Energy*, 1960, **4**, 1–19.
17. Kreith, F. and Kreider, J. F., *Principles of Solar Engineering*, New York, McGraw-Hill, 1978.
18. He, H. L., Yu, G. R. and Niu, D., Method of global solar radiation calculation on complex territories. *Resour. Sci.*, 2003, **25**(1), 78–85 (in Chinese).
19. Unger, J., Connection between urban heat island and sky view factor approximated by a software tool on a 3D urban database. *Int. J. Environ. Pollut.*, 2009, **36**, 59–80.
20. Nichol, J. E. and Wong, M. S., Spatial variability of air temperature over a city in a winter night. *Int. J. Remote Sens.*, 2008, **29**(24), 7213–7223.
21. Wong, M. S. *et al.*, A simple method for designation of urban ventilation corridors and its application to urban heat island analysis. *Build. Environ.*, 2010, **45**, 1880–1889.

ACKNOWLEDGEMENTS. This research was supported by the National Natural Science Foundation of China (41401471, 41571418, 41201369) and the Priority Academic Program Development of Jiangsu Higher Education Institutions. The authors gratefully acknowledge Dr Huade Guan and Dr Simon Bengler from School of the Environment, Flinders University for providing data and invaluable comments.

Received 15 July 2015; revised accepted 11 October 2015

doi: 10.18520/cs/v110/i4/619-626